

Synthesis of silicate clay minerals-based novel Mt/YF₃:Eu³⁺ nanocomposites for regulated luminescent intensity-quantum yield-fluorescence lifetime

Hongxia Peng^{a,*}, Weicai Peng^a, Jingyou jiang^a, Huibin Shi^a, Juan Zhu^a, Junna Xu^a, Fabiao Yu^{b,c,**}

^a Hunan Provincial Key Laboratory of Fine Ceramics and Powder Materials, Hunan University of Humanities, Science and Technology, Lou'di, Hunan, 417000, PR China

^b Key Laboratory of Hainan Trauma and Disaster Rescue, The First Affiliated Hospital of Hainan Medical University, Hainan Medical University, Haikou, 571199, China

^c Engineering Research Center for Hainan Bio-Smart Materials and Bio-Medical Devices, Key Laboratory of Emergency and Trauma, Ministry of Education, Key Laboratory of Hainan Functional Materials and Molecular Imaging, College of Emergency and Trauma, Hainan Medical University, Haikou, 571199, China

ARTICLE INFO

Handling Editor: Dr P. Vincenzini

Keywords:

Montmorillonite nanosheet

YF₃:Eu³⁺

Luminescent intensity

Quantum yield

Lifetime

ABSTRACT

Rare earth luminescent materials have broad application prospects in the fields of white light LED lighting, flat panel display, biological imaging and so on. Here, we developed a novel silicate clay minerals-based montmorillonite nanosheet(Mt)/YF₃:Eu³⁺ nanocomposites with strong luminescence performance. Mt carrier plays a three role: (1) reducing the size and improving dispersion of YF₃:Eu³⁺ nanoparticles by surface effect; (2) narrowing down the band gap and increasing Urbach tail energy by interface effect; (3) reducing the shielding of the hole-electron Coulomb interactions while improving the exciton binding energy of YF₃:Eu³⁺, thus improving the radiative recombination by dielectric effect. Therefore, orthogonal phase YF₃:Eu³⁺ nanoparticles (diameter 20~140 nm) binding to the surface of Mt via chemical bond interactions. The combination of Mt and YF₃:Eu³⁺ not only enhanced luminescent intensity (about 2 times) but also improved the quantum yield (0.14% to 0.4%) and fluorescence lifetime (0.338 ns to 0.405 ns) of YF₃:Eu³⁺ nanoparticles at 595 nm. In addition, the combination of Mt and YF₃:Eu³⁺ give luminescent properties to Mt thereby improving the utilization rate of Mt and YF₃:Eu³⁺ nanoparticles. It was found that the research supplies an insight on the development of new type luminescent materials, and hopefully it could promote them application in many fields.

1. Introduction

Rare earth phosphors for white light LED have several remarkable advantages such as narrow band emission, which can be concentrated in a specific wavelength range, good stability at short ultraviolet (185 nm) radiation, and high emission intensity at high temperature. Among, YF₃:Eu³⁺ is a superior red phosphor due to its low refractive index, good chemical stability, non-hygroscopicity and insoluble [1,2]. However, it has many disadvantages, for instance, shorter fluorescence lifetime, lower fluorescence quantum yield and utilization rate [3].

For the moment, the usual methods to improve the luminescence property of rare earth luminescent materials mainly include coating method, ion doping method and introducing surface plasma resonance

effect method, but these methods still have many different defects. Coating method is effective method to improve the luminescence properties of rare-earth luminescent materials. By coating a homogeneous or heterogeneous shell on the surface of the material to reduce the surface defects of the material, increase the distance of the luminescence center, and reduce the surface fluorescence quenching to improve its luminescence intensity [4–8]. However, almost all the coating methods face a common problem, which is difficult to effectively control the thickness. Ion doped method is another effective method to improve the luminescence properties of rare-earth luminescent materials. The local symmetry of matrix lattice is adjusted by ion doping (e. g., Fe³⁺) to improve the emission intensity of the rare-earth luminescent materials. However, it's hard to control accurately the content of doping elements

* Corresponding author.

** Corresponding author. Key Laboratory of Hainan Trauma and Disaster Rescue, The First Affiliated Hospital of Hainan Medical University, Hainan Medical University, Haikou, 571199, China.

E-mail addresses: 3197@huhst.edu.cn (H. Peng), yufabiao@hainmc.edu.cn (F. Yu).

<https://doi.org/10.1016/j.ceramint.2023.08.115>

Received 28 June 2023; Received in revised form 6 August 2023; Accepted 10 August 2023

Available online 11 August 2023

0272-8842/© 2023 Elsevier Ltd and Techna Group S.r.l. All rights reserved.

and the replacement position of target atoms. And the coexistence of multiple doped ions with high concentration will cause cross-relaxation, which can lead to fluorescence quenching. In addition, the emission intensity of rare-earth luminescent materials can be enhanced by coupling resonance energy transfer with surface plasmon materials, such as gold and silver, WO_{3-x} and Cu_{2-x}Se [9–12]. However, the price of gold and silver is higher, and the morphology and defect concentration of WO_{3-x} and Cu_{2-x}Se are difficult to control [13]. Al_2O_3 and SiO_2 nanoparticles, as commonly used dielectric materials, can improve the luminescence intensity of the rare earth fluoride luminescent materials [14,15]. However, they have lower dielectric constant ratio with the nano-materials due to their charge transfer and rotation, it is difficult to efficient enhancement of the surface and internal local fields of the rare earth fluoride luminescent materials. And the dielectric constant of Al_2O_3 and SiO_2 nanoparticles can only be controlled by changing their porous structure. At the same time, the porous structure and its void size not easy to control, which limits their practical application in the field of optical materials. Montmorillonite (Mt, $\text{Al}_2\text{O}_9\text{Si}_3$, dielectric constant 16.1–38.2) nano-sheet is a class of negatively charged silicate sheets of nanothickness [16,17]. Mt nano-sheet is a kind of sheet-like silicate clay mineral with mortal specific surface area, up to 700–800 m^2/g [18]. The interface interaction of the Mt nano-sheet and loaded materials can not only change the electronic structures, exciton binding energy and band gaps of the loaded materials, but also effectively adjusts the size, morphology and dispersion of the loaded materials [19–23]. Its high dielectric constant ratio are adjusted by the concentration of the loaded materials. Mt is natural formation, extensive resources, complete shape, low price and low toxicity. Mt is a good silicate clay minerals assembly of nano-functional materials. For example, a new type of CeO_2 @MMT nanoenzyme-targeted therapeutic drug was successfully synthesized.

Cerium oxide nanoparticles (CeO_2 NPs) were grown in situ on montmorillonite (MMT) for inflammatory sites. By binding to MMT, CeO_2 NPs significantly inhibited the absorption phenomenon in the whole body, reduced its potential nanotoxicity, and also give photodynamic activity to MMT [24]. A new nanocomposite composed of nano-structured minerals (Montmorillonite), starch particles and liquid metals was reported. The new nanocomposites have chemical, optical and mechanical response property. They has write-wipe capabilities in electrical filed, and also enhance microbial culture/biofilm growth in vitro and biofuel production [25]. Guan et al. designed and synthesized a unique fluorescent surfactant, which combines the properties of the aggregation-induced emission (AIE) and amphiphilicity, to image macrodispersion of montmorillonite (Mt) and layered double hydroxide fillers in polymer matrix. The proposed fluorescence imaging provides a number of important advantages over electron microscope imaging, and opens a new avenue in the development of direct three-dimensional observation of inorganic filler macrodispersion in organic–inorganic composites [26].

We combined the beneficial properties of Mt nanosheet and $\text{YF}_3:\text{Eu}^{3+}$ to synthesize a new type of silicate clay minerals-based Mt/ $\text{YF}_3:\text{Eu}^{3+}$ nanocomposites (Fig. 1). A combination of Mt nanosheet and $\text{YF}_3:\text{Eu}^{3+}$ not only endows Mt with luminescent properties but also effectively improves the luminescent performance of $\text{YF}_3:\text{Eu}^{3+}$ nanoparticles by regulate their size, exciton binding energy and band gaps. This research render a new policy for improving the utilization rate and optimizing performance of Mt nanosheet and $\text{YF}_3:\text{Eu}^{3+}$ nanoparticles.

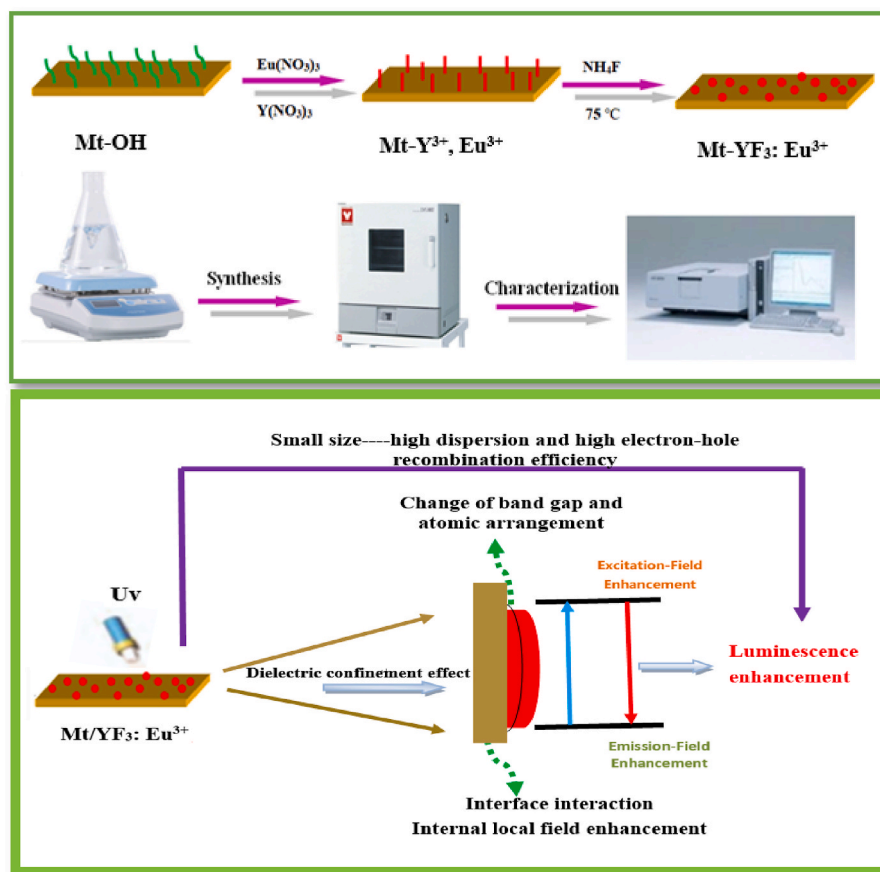


Fig. 1. Synthesis procedure and schematic illustration of luminescence enhancement mechanism of Mt/ $\text{YF}_3:\text{Eu}^{3+}$ nanocomposites.

2. Experimental sections

2.1. Preparation of Mt/YF₃:Eu³⁺ nanocomposites

Mt (0.25 g) was dispersed in deionized water (25 mL), and Y(NO₃)₃ (1.6 mL, 0.4 mol/L) and Eu(NO₃)₃ (0.6 mL, 0.4 mol/L) were added. After ultrasonic dispersion for 10 min, NH₄F (5 mL 0.6 mol/L) solution was added and then heated to 80 °C. After magnetic stirring for 1 h, the deposit washed six times with deionized water and ethanol, and dried at 80 °C for 3 h. Finally, Mt/YF₃:Eu³⁺ nanocomposites were prepared.

2.2. Preparation of YF₃:Eu³⁺ nanoparticles

Deionized water (25 mL) was mixed with Y(NO₃)₃ (1.6 mL, 0.4 mol/L) and Eu(NO₃)₃ (0.6 mL, 0.4 mol/L) solution. After ultrasonic dispersion for 10 min, NH₄F (5 mL 0.6 mol/L) solution was added and heated to 80 °C. After magnetic stirring for 1 h, the deposit washed six times with deionized water and ethanol for several times, and dried at 80 °C for 3 h. Finally, YF₃:Eu³⁺ nanoparticles were prepared.

2.3. Reagents and characterization

All reagents used were of analytical grade and used without further purification. Mt was purchased from Xin Cheng Shen Fei Aluminum Alloy Co., Ltd. (Wenzhou, China). Ammonium fluoride (NH₄F) was purchased from Beijing Chemical Works. Y(NO₃)₃ and Eu(NO₃)₃ were purchased from Science and Technology Parent Company of Changchun Institute of Applied Chemistry.

X-ray diffraction (XRD) patterns of the samples were measured using an AXS D8 Advance diffractometer (Bruker, Bremen, Germany) with Cu K α radiation ($\lambda = 0.15406$ nm) at 40 kV and 40 mA. Scanning electronic microscopy (SEM) images were recorded on a Hitachi S-4800 microscope. Transmission electron microscopy (TEM), EDS, HRTEM and SAED (FEI, Tecnai T20, Netherland) were carried out after dissolving all samples in ethanol and mounted them in a copper grid. The valence states of the elements were analyzed by X-ray photoelectron spectroscopy (XPS) Thermo Scientific K-Al pha+. The X-ray source was Al K α micro-focusing monochromatic source which the beam spot was continuously adjustable from 30 to 400 μ m, and the step size was 5 μ m. The photoluminescence (PL) excitation and emission spectra were recorded on a Hitachi F-4500 spectrofluorimeter equipped with a 150 W xenon lamp as the excitation source. Fluorescence lifetime and quantum yield were measured by Edinburgh FLS1000 fluorescence spectrophotometer. The UV/Vis/Infrared light absorption performance was analyzed by UV 3600 spectrometer with a scanning range of 700~200 nm. A Bruker Vertex 70 infrared spectrometer was used for FTIR analysis with a scanning range of 4000~400 cm⁻¹. Agilent 4294A impedance analyzer was used for dielectric constant and dielectric loss analysis with room temperature.

3. Results and discussion

Fig. 2 shows the XRD patterns of Mt, YF₃:Eu³⁺ and Mt/YF₃:Eu³⁺ nanocomposites. From the spectrum line of Mt, the diffraction peaks appeared at 19.84°, 20.83°, 26.66°, 28.44°, 44.97°, 46.20°, 54.90°. The position and relative intensity of the diffraction peaks are consistent with standard card of the monoclinic phase Mt (PDF#29-1487), indicating that the sample is monoclinic phase Mt. From the patterns of YF₃:Eu³⁺, the diffraction peaks appear at 26.23°, 28.38°, 44.90°, 46.22°, 52.23°. The position and relative intensity of the diffraction peaks are consistent with the standard card of orthogonal phase of YF₃:Eu³⁺ (PDF#05-0392). It can be seen from the XRD spectrum of Mt/YF₃:Eu³⁺ nanocomposite that the characteristic reflections correspond to the monoclinic phase ($2\theta = 19.84^\circ, 20.83^\circ, 26.66^\circ, 28.44^\circ, 44.97^\circ, 46.20^\circ, 54.90^\circ$) of Mt (JCPDS. 29-1487), and the orthogonal phase ($2\theta = 26.23^\circ, 28.38^\circ, 44.90^\circ, 46.22^\circ, 52.23^\circ$) of YF₃:Eu³⁺ (JCPDS. 05-0392),

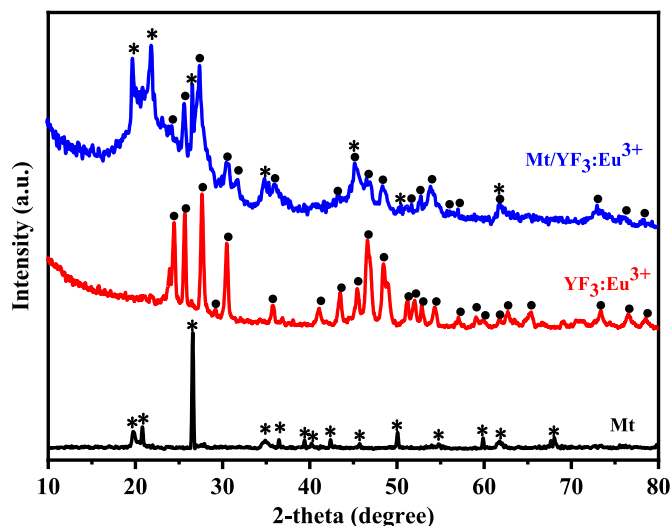


Fig. 2. XRD patterns of Mt, YF₃:Eu³⁺ and Mt/YF₃:Eu³⁺ nanocomposites.

which indicating that the nanocomposite consists of Mt and YF₃:Eu³⁺. Moreover, through the XRD spectrum comparison of the three samples, it is found that the relative intensity of the diffraction peaks of Mt and YF₃:Eu³⁺ is significantly weakened, and even some peaks disappear. The main reason is that YF₃:Eu³⁺ was coated on Mt, which reduces the relative intensity of the diffraction peaks of Mt. Analysis shows that the final product is composed of Mt and YF₃:Eu³⁺.

It can be seen from Fig. 3a,b, Mt has nano-sheet structure with a smooth surface and stacked in layers. After YF₃:Eu³⁺ nanoparticles deposition onto the surface of Mt, Mt/YF₃:Eu³⁺ nanocomposites preserved nano-sheet shapes (Fig. 3c and d). The surface roughness and looseness of Mt/YF₃:Eu³⁺ nanocomposites increases compared to Mt (Fig. 3d). And as can be seen from Fig. 3c and d, many nanoparticles with mean sizes of 82.43 nm ($n = 100$) are deposited on the Mt surface. Compare to independent and scattered YF₃:Eu³⁺ nanoparticles (Fig. 3e and f), the size of YF₃:Eu³⁺ nanoparticles on the surface of Mt is obviously reduced (Fig. 3d). The growth and aggregation of YF₃:Eu³⁺ were inhibited due to two-dimensional limited surfaces of Mt nanosheet. The result shows that Mt can adjust the sizes and dispersion of YF₃:Eu³⁺ nanoparticles through its specific surface (see Fig. 3d).

As shown in Fig. 4a, multiple YF₃:Eu³⁺ nanoparticles are wrapped on the surface of Mt. The Y³⁺ and Eu³⁺ ions are adsorbed on the negatively charged surface of Mt, and then YF₃:Eu³⁺ undergo nucleation and growth on the surface of Mt (Fig. 1). The TEM image of Mt/YF₃:Eu³⁺ nanocomposite (Fig. 4a) clearly shows that YF₃:Eu³⁺ nanoparticles are deposited on the surface of Mt. The HRTEM image of Mt/YF₃:Eu³⁺ nanocomposite shows that the lattice spacing values were 0.312 and 0.343 nm, respectively, corresponds to the (111) and (020) plane of YF₃:Eu³⁺, which approved that the nanoparticles were YF₃:Eu³⁺ crystals (Fig. 4b). The inset in Fig. 4b (SAED patterns of the Mt/YF₃:Eu³⁺ nanocomposite) showed polycrystalline diffraction rings and discrete diffraction spots, which suggests that the nanocomposite is polycrystalline. Fig. 4c-i are the distribution map of O, Mg, Eu, Si, Ai, F and Y. All of the elements were uniformly distributed. TEM and EDX analysis further confirmed the formation of the Mt/YF₃:Eu³⁺ nanocomposites (see Fig. 4).

It can be seen from the infrared spectra (Fig. 5) of Mt, the H-O-H stretching vibration peaks emerged at 3200~3600 cm⁻¹ [18]. The deformation vibration absorption peak of H₂O emerged at 1637 cm⁻¹. The absorption peaks at 1030 and 900 cm⁻¹ come from the telescopic vibration band of the -Si-O- bond. The absorption peaks at 795 and 500~600 cm⁻¹ were attributed to the vibration bands of Si-O-Si and O-Si, respectively [19]. It can be seen from the infrared spectra of YF₃:Eu³⁺, the absorption peak at 3250-3600 cm⁻¹ can be the result of H-O-H

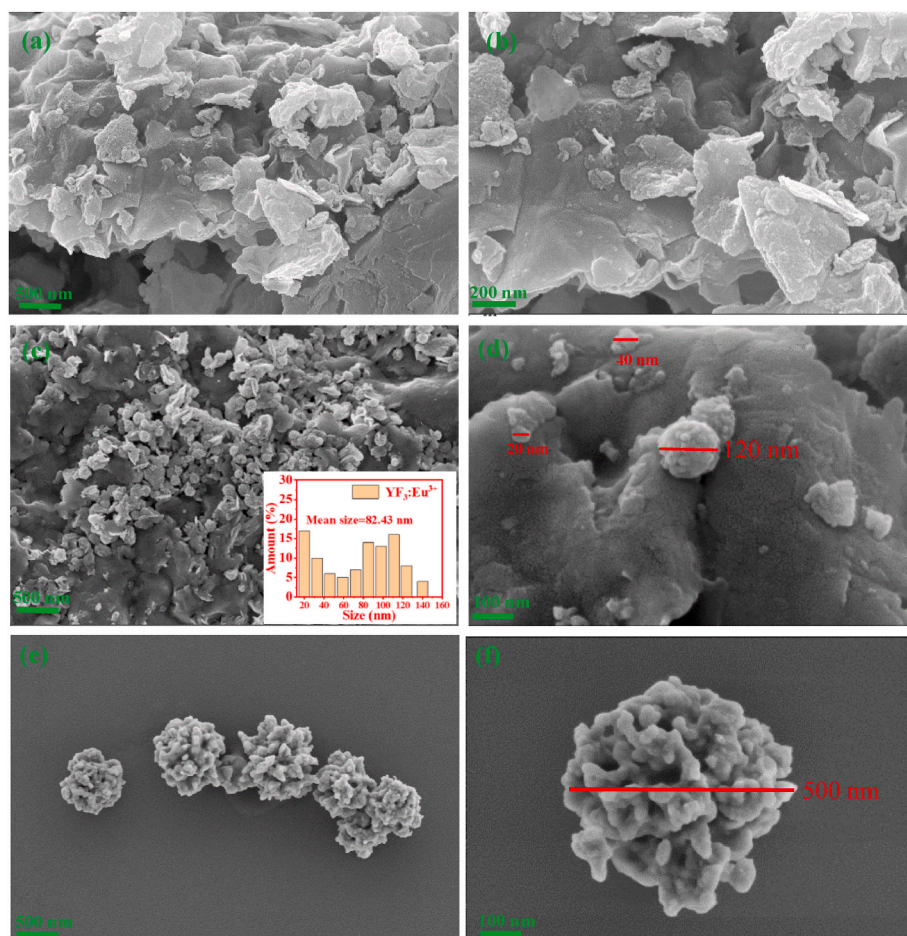


Fig. 3. SEM of Mt (a, b), Mt/YF₃:Eu³⁺ and (inset) corresponding particle size distribution histogram (c, d), YF₃:Eu³⁺ (e, f).

stretching vibration peak. The absorption peak at 1637, 1401 and 1424 cm⁻¹, respectively, can be the result of the bending vibration absorption peaks of H–O–H and the vibration absorption peaks of NO₃ appeared [27]. The absorption peaks at 1045 and 808 cm⁻¹ can be the result of the absorption peaks of C–O (CO₂) [28].

In the spectrum (Fig. 5) of Mt/YF₃:Eu³⁺, three absorption peaks appears at 3622, 3430 and 3120 cm⁻¹ can be the result of the stretching and bending vibration absorption of –OH [28]. The absorption peaks at 1030 and 1035 cm⁻¹ came from the stretching vibration absorption peak of the Si–O–Si bond [29]. The absorption peak at 795 cm⁻¹, 619 cm⁻¹ and 523 cm⁻¹ put down to the flexural vibration absorption of Si–O, Al–O–Si and Mg–O, respectively [17,29]. Compared with the spectra of Mt and YF₃:Eu³⁺, H–O–H stretching vibration peak at 3430 cm⁻¹ and the NO₃ vibration absorption peak at 1401 cm⁻¹ in the spectra of Mt/YF₃:Eu³⁺ nanocomposite were attenuated. Which proved that YF₃:Eu³⁺ was successfully coated on the surface of Mt. When YF₃:Eu³⁺ nanoparticles was coated on the surface of Mt, which eliminated or degraded the active groups of the surface of YF₃:Eu³⁺, thereby its emission intensity was boosted.

The XPS full spectrum of Mt, YF₃:Eu³⁺ and Mt/YF₃:Eu³⁺ nanocomposite shown in Fig. 6a. The full spectrum of the Mt/YF₃:Eu³⁺ nanocomposite showed the nanocomposite comprise of Si, Al, Mg, Eu, Y, O, and F elements. Besides that, the high-resolution XPS spectra of O 1s, Si 2p, Al 2p, Mg 1s, Y 3d, Eu 3d, and F 1s were also collected to analyze the chemical environments of these atom. After YF₃:Eu³⁺ deposition onto the surface of Mt, the binding energies of Si 2p and Al 2p reduced from 103.57 to 75.40 to 103.24 and 74.90 eV, respectively (Fig. 6b and c), indicating the coupling of YF₃:Eu³⁺ on Mt nanosheet.

The change in the spectra of Eu 3d, Y 3d, and F 1s could also explain the interaction between YF₃:Eu³⁺ and Mt nanosheets. Before YF₃:Eu³⁺ deposition onto the surface of Mt, the spectrum of Eu 3d appeared two spectrum peak at 1158.0 eV and 1167.6 eV. After YF₃:Eu³⁺ deposition onto the surface of Mt, the two spectrum peak of Eu 3d are blue shift, respectively. This is due to changes in the electron binding energy of the Eu inner shell, which show that the bonding interactions (Mt–O–Eu³⁺) may generated at the interface between Mt–O and Eu³⁺ (Fig. 6E). Fig. 6F shows Y 3d peak for pure YF₃:Eu³⁺ and Mt/YF₃:Eu³⁺. The Y 3d peak appears at around 161.0 and 163.0 eV in YF₃:Eu³⁺. The blue shift of peak of Y 3d at 163.0 and 161.0 eV could be caused by Y–O–Mt bond generated. Notably, the spectrum of Mt/YF₃:Eu³⁺ shows a new peak at 154.2 eV, which may be due to the formation of Y–O–Mt between YF₃:Eu³⁺ and Mt (O atom in Mt). After the YF₃:Eu³⁺ coated on the surface of Mt nanosheet, the peaks of O 1s blue shifted to the lower binding energy compared to YF₃:Eu³⁺, indicating the electron cloud density and electronegativity of O atom decrease (see Fig. 6G). The results are further illustrated the interactions between Mt and YF₃:Eu³⁺. At the same time, the binding energies of F 1s decreased from 687.5 to 685.8 eV (Fig. 6H), suggesting the bonding of YF₃:Eu³⁺ on the surface of Mt. It was further confirmed that the YF₃:Eu³⁺ is coated on the surface of Mt nanosheet by combining the analysis of TEM elemental mapping, IR, and XPS.

In the excitation spectra (Fig. 7A), which were monitored with 595 nm emission of Eu³⁺, we observed a strong excitation peak at 395 nm that can be assigned to the energy level transition of ⁷F₀–⁵L₆ of Eu³⁺. The emission spectra (Fig. 7B) were obtained by excitation at 397 nm, the strongest emission peak (at 595 nm) was attributed to the ⁵D₀–⁷F₁ forced electric dipole transition. The other emission bands observed at 616 nm was attributed to ⁵D₀–⁷F₂ transition. Compared with YF₃:Eu³⁺,

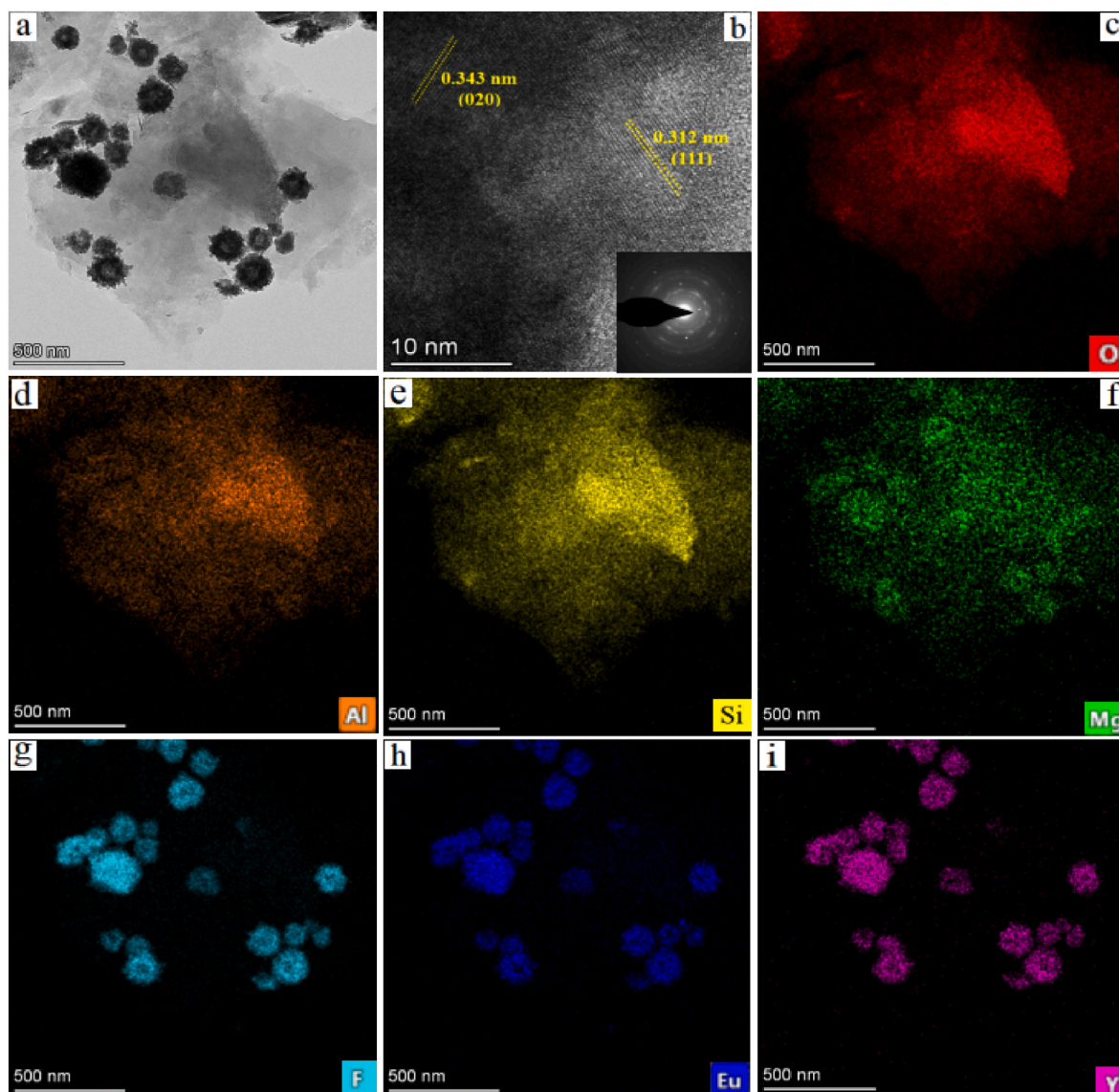


Fig. 4. (a) TEM image of Mt/YF₃:Eu³⁺ nanocomposite; (b) HRTEM image and the SAED pattern of Mt/YF₃:Eu³⁺ nanocomposite; (c–i) Energy Dispersive X-ray (EDX) mapping of Mt/YF₃:Eu³⁺ nanocomposite.

the emission intensity of Mt/YF₃:Eu³⁺ notably enhanced (about 2 times), as shown in Fig. 7B. Usually, a single luminescence center is a symmetric peak structure [21]. So in Mt/YF₃:Eu³⁺ nanocomposite, Eu³⁺ is a single luminescence center that occupies only one lattice position. Eu³⁺ does not replace different cations or enters into different lattices, thus not forming a variety of light-emitting centers with different surrounding lattice environments. And the quantum yield of Mt/YF₃:Eu³⁺ and YF₃:Eu³⁺ was also measured, which was 1.4% and 0.4%, respectively. This proves that the energy conversion ability to the absorbing photons of Eu³⁺ is enhanced by Mt.

The decay curves of the prepared YF₃:Eu³⁺ and Mt/YF₃:Eu³⁺ nanocomposite were showed in Fig. 8. The fluorescence decay curves of YF₃:Eu³⁺ and Mt/YF₃:Eu³⁺ nanocomposite conform to the dual-exponential decay behavior, and the dual exponential function is adopted [21]:

$$I(t) = \alpha_1 e^{(-t/\tau_1)} + \alpha_2 e^{(-t/\tau_2)} \quad (1)$$

Where I is the fluorescence intensity, τ_1 and τ_2 are the fast process and slow process of fluorescence decay, α_1 and α_2 are the fitting index of the two processes. Its average fluorescence lifetime (s) is calculated by formula (2):

$$\tau = (\alpha_1 \tau_1^2 + \alpha_2 \tau_2^2) / (\alpha_1 \tau_1 + \alpha_2 \tau_2) \quad (2)$$

Based on formula (2), the fluorescence lifetime of YF₃:Eu³⁺ and Mt/YF₃:Eu³⁺ nanoparticles is 0.338 ns and 0.405 ns, separately. It can be seen from Fig. 8 that the fluorescence lifetime of the Mt/YF₃:Eu³⁺ nanoparticles is longer than that of YF₃:Eu³⁺ nanoparticles. It is well known that the microscopic properties and processes such as band gap, energy levels and carrier migration of luminescent nanomaterials may influence their luminescence properties.

The optical absorption abilities and band gap of Mt and Mt/YF₃:Eu³⁺ nanocomposite were measured by DRS in Fig. 9. Fig. 9a shows the comparison of UV–vis optical absorption characteristics of pure YF₃:Eu³⁺, Mt and Mt/YF₃:Eu³⁺. It can be observed that the optical absorption capacity of Mt/YF₃:Eu³⁺ is higher than that of Mt and YF₃:Eu³⁺ at 300–800 nm, indicating that the Mt/YF₃:Eu³⁺ nanocomposite possessed unique optical properties. Compared to that of Mt and YF₃:Eu³⁺, the absorption edge of Mt/YF₃:Eu³⁺ nanocomposite has an obvious red shift, which can be attributed to the dielectric confinement effect in Mt/YF₃:Eu³⁺ nanocomposite. Because the dielectric confinement effect can enhance the Coulomb force between electronics and holes, thus enhancing the binding energy between electron-hole pairs, while

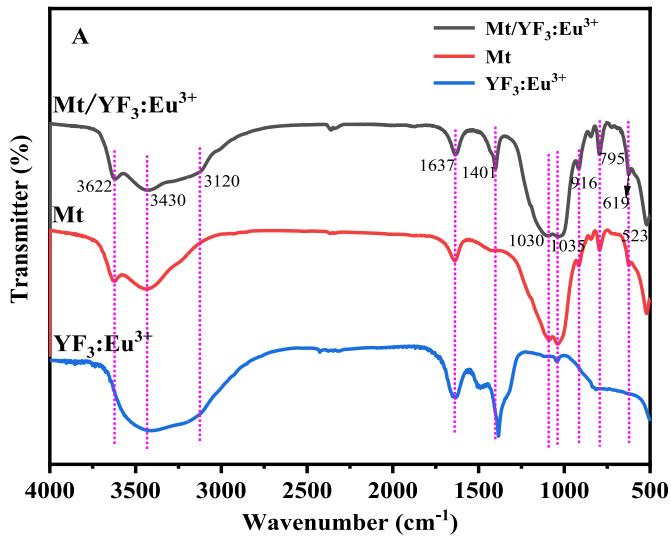


Fig. 5. Infrared spectrum of Mt, YF₃:Eu³⁺ and Mt/YF₃:Eu³⁺ nanocomposite.

weakening the spatial confinement energy between electron-hole pairs, thus causing the redshift phenomenon. The dielectric confinement effect is large, the greater the redshift of the absorption spectrum. As shown in Fig. 9B-D, the energy band gap of the Mt/YF₃:Eu³⁺ nanocomposite was approximately 2.87 eV, which was significantly narrower than that of YF₃:Eu³⁺ (3.92 eV) and Mt (3.50 eV). This band gap made the Mt/YF₃:Eu³⁺ nanocomposite to adsorb light in the UV–vis region. The effect of Mt on the band gap of YF₃:Eu³⁺ nanoparticles put down to the synergistic action of the surface and interface. XRD results analysis showed the low crystallinity of YF₃:Eu³⁺ in the nanocomposites. The low crystallinity increased crystal defects. The growth of these defects would generate the defect energy level, and defects dispersed and overlapped with the edge of the conducting band [19]. These effects led to the narrowing of the band gap of the YF₃:Eu³⁺ nanoparticles on the surface of Mt. This result is consistent with that obtained by UV absorption spectroscopy. The obvious influence of Mt nanosheet on the band gap of YF₃:Eu³⁺ nanoparticles may also be associated with interface defects. In Mt/YF₃:Eu³⁺ nanocomposite, the increasing concentration of the interface defects leads to the overlap of the wave functions in the defect state, thus dividing the separated defect energy levels into energy bands [20]. The width of the defect energy band is proportional to the defect concentration [20,30]. The wide defect band led to the overlapping of defect band with the conduction band, and move the conduction band down thus narrow the band gap (see Fig. 9).

In order to further prove the increase of local defect state and the change of material structure disorder, Urbach tail energy by using equation (3) was calculated. Urbach tail energy of YF₃:Eu³⁺ nanoparticles and the Mt/YF₃:Eu³⁺ nanocomposite were 0.266, and 0.567 eV, respectively (Fig. 10).

$$\alpha(\nu) = \alpha_0 \exp \frac{h\nu}{E_u} \alpha(\nu) = \alpha_0 \exp \frac{h\nu}{E_u} \quad (3)$$

where α is absorption coefficient, α_0 is a constant, h is the Planck constant, ν is the frequency of photon, and E_u is the Urbach tail energy. The value was calculated from the inverse of the slope by using the plot of $\ln(\alpha)$ and $h\nu$.

α can be obtained from formula (4)

$$\alpha = 2.303 \times \frac{A}{t} \quad (4)$$

Where A is the light absorption intensity and t is the thickness of the samples.

The definition of Urbach tail energy showed that the material with

high or low Urbach energy has a certain amount of defect states. Compared to YF₃:Eu³⁺ nanoparticles, Urbach energy of Mt/YF₃:Eu³⁺ nanocomposite obviously higher, which indicate that the interface of Mt and YF₃:Eu³⁺ have the large defect states density. Therefore, according to the Urbach energy values, Mt can act as a good carrier for YF₃:Eu³⁺ nanoparticles, and the luminescence performance of YF₃:Eu³⁺ nanoparticles can be enhanced by changing in the crystal field.

The dielectric confinement effects is caused by the mismatch of dielectric constants between nanoparticles and its surrounding. It can improve the dielectric properties due to the enhancement of the surfaces and inside local fields of nanoparticles. Dielectric constant and dielectric loss are two index for appraising the dielectric properties of nanomaterials. In a luminescent nanocomposite, the luminescence performance can be well regulated by the dielectric confinement effect [18].

Previous research reports showed [17], the dielectric constant of Mt is less than 5.00, and the dielectric loss is less than 0.002. As shown in Fig. 11, the dielectric constant of YF₃:Eu³⁺ nanoparticles was less than 50.00, and the dielectric loss was less than 3.00. As frequency is abated, its dielectric constant and dielectric loss does not change significantly. It can see in Fig. 11, the dielectric constant and dielectric loss of the Mt/YF₃:Eu³⁺ nanocomposite improved. Which is that the interface polarization effect occurs at the interface of Mt and YF₃:Eu³⁺, so raised the accumulation of electrons at the interface. As frequency increased, the dielectric constant and dielectric loss factor gradually decreased. The results showed that the interface of Mt/YF₃:Eu³⁺ nanocomposite produced a strong dielectric confinement effect, thus will optimized the luminescence property of the Mt/YF₃:Eu³⁺ nanocomposite.

It has been shown that the exciton binding energy can be regulated by dielectric confinement effect. The difference in the dielectric constant between the rare earth luminescent material (YF₃:Eu³⁺) and the mineral carrier (Mt nanosheet) will increase the influence of the dielectric confinement effect on the exciton binding energy [31]. Mt with low dielectric constant and less polarizable reduces the shielding effect of the hole-electron Coulomb interaction of YF₃:Eu³⁺, resulting in an increase of the exciton binding energy of YF₃:Eu³⁺. Theoretically, the correlation among E_b of 3D (3 Dimensions) excitons and dielectric constant of 2D (2 Dimensions) carrier, is expressed by the following equation [32]:

$$E_b^{3D} = \frac{1}{4} \left(\frac{\epsilon_w}{\epsilon_b} \right)^{-2} E_b^{2D} \quad (5)$$

where ϵ_w and ϵ_b are the dielectric constants of YF₃:Eu³⁺ luminescent material and Mt nanosheet, respectively. E_b^{3D} represent the exciton binding energy of the corresponding 3D rare earth luminescent material. E_b^{2D} represent the exciton binding energy of the corresponding

2D Mt carrier. According to eq. (5), the increase in ϵ_b and or the decrease in ϵ_w would lead to an increase in the 3D exciton binding energy. The luminescent intensity of YF₃:Eu³⁺ nanoparticles may thus be further enhanced by enlarging the dielectric contrast between the YF₃:Eu³⁺ nanoparticles and Mt.

According to the above analysis, the main reasons for the Mt-enhanced YF₃:Eu³⁺ luminescence performance are as follows: (1) Mt could weakened or reduced the surface lattice distortion, surface group, and surface defects of YF₃:Eu³⁺, so removed the surface negative effects of the luminescence properties of Mt/YF₃:Eu³⁺ nanocomposite thereby improved the luminescence intensity and quantum yield of YF₃:Eu³⁺. At the same time, it can eliminate the interference of the external environment to Eu³⁺, then enhance the emission intensity of YF₃:Eu³⁺. And more importantly, the surface confinement effect of Mt reduced the particle size of YF₃:Eu³⁺ nanoparticles and improved dispersibility. The changing of the surface state (the decreasing of particle size and increasing of surface area) of YF₃:Eu³⁺ nanoparticles enhanced significantly the emission intensity of Mt/YF₃:Eu³⁺ nanocomposite. (2) It can be seen from the results of the band gap and Urbach tail energy, the interface effect between Mt and YF₃:Eu³⁺ nanoparticles narrowed down the band gap and increased local defect state at interface, thereby

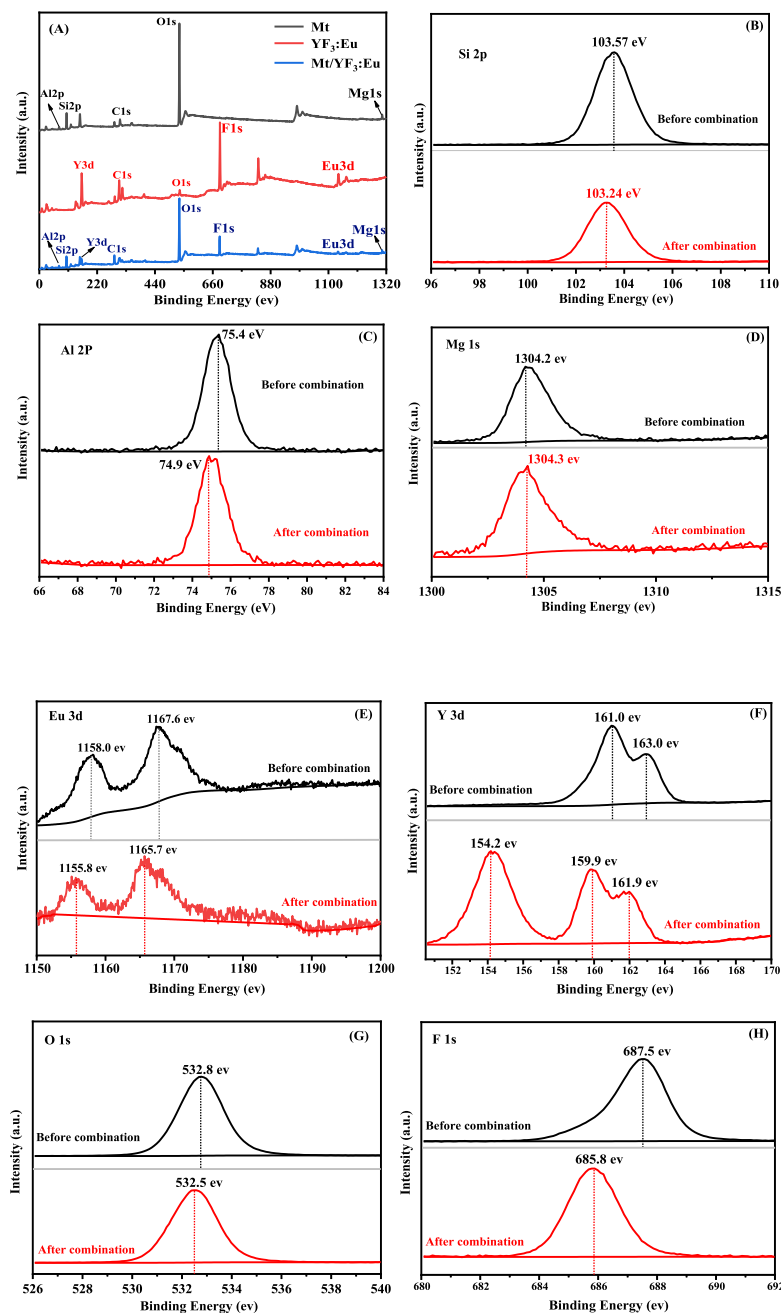


Fig. 6. XPS spectra (A) XPS survey spectra of Mt, $\text{YF}_3:\text{Eu}^{3+}$ and $\text{Mt}/\text{YF}_3:\text{Eu}^{3+}$ nanocomposite and High-resolution Si 2p (B), Al 2p (C), Mg 1s (D), Eu 3d (E), Y 3d (F), O 1s (G), F 1s (H).

change the crystal field of Eu^{3+} which could lead to boosted the luminescence intensity of $\text{Mt}/\text{YF}_3:\text{Eu}^{3+}$ nanocomposite. (3) When the difference between the dielectric constant of Mt and $\text{YF}_3:\text{Eu}^{3+}$ is large, the dielectric confinement effect is stronger. The analytic result of dielectric performance showed that the interface of $\text{Mt}/\text{YF}_3:\text{Eu}^{3+}$ nanocomposite produced a strong dielectric confinement effect. The dielectric confinement effect enhanced the hole-electron Coulomb interactions while improved the exciton binding energy and oscillator strength, thereby enhanced the luminescence intensity of $\text{Mt}/\text{YF}_3:\text{Eu}^{3+}$ nanocomposite. At the same time, the dielectric confinement effect is weakened the spatial domain energy between the electron-hole pair (the main factor producing the quantum size effect), that is, the energy changing caused by the surface effect is greater than that caused by the

space effect, so that the energy band gap is reduced. The dielectric confinement effect can effectively improve the exciton recombination rate thereby improve the luminescence intensity. However, the higher electron-hole Coulomb force caused by the strong dielectric confinement effect will seriously affect the local homogeneity of the carrier inside the material; it will also rapidly enrich the carriers, and then the local carrier concentration of $\text{Mt}/\text{YF}_3:\text{Eu}^{3+}$ nanocomposite is higher than $\text{YF}_3:\text{Eu}^{3+}$ at the same excitation intensity. Moreover, dielectric confinement effect can also significantly affect the Auger recombination rate of $\text{Mt}/\text{YF}_3:\text{Eu}^{3+}$ nanocomposite, which can regulate the quantum yield and fluorescence lifetime [33]. Auger recombination refers to the corresponding recombination process of Auger transition. Auger effect is a three-particle effect. When electrons and hole recombination, the energy

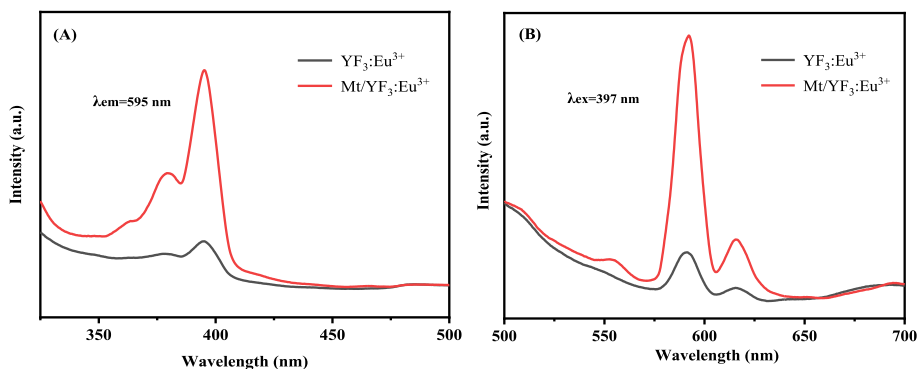


Fig. 7. Fluorescence spectra of Mt/YF₃:Eu³⁺ nanocomposites: Excitation (A) and emission (B) spectra of Mt/YF₃:Eu³⁺ and YF₃:Eu³⁺.

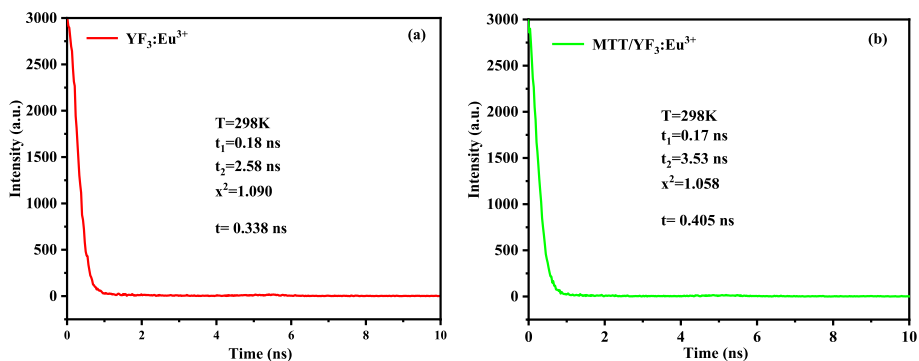


Fig. 8. Fluorescent decay curves of ⁵D₀-⁷F₂ (595 nm) for Eu³⁺.

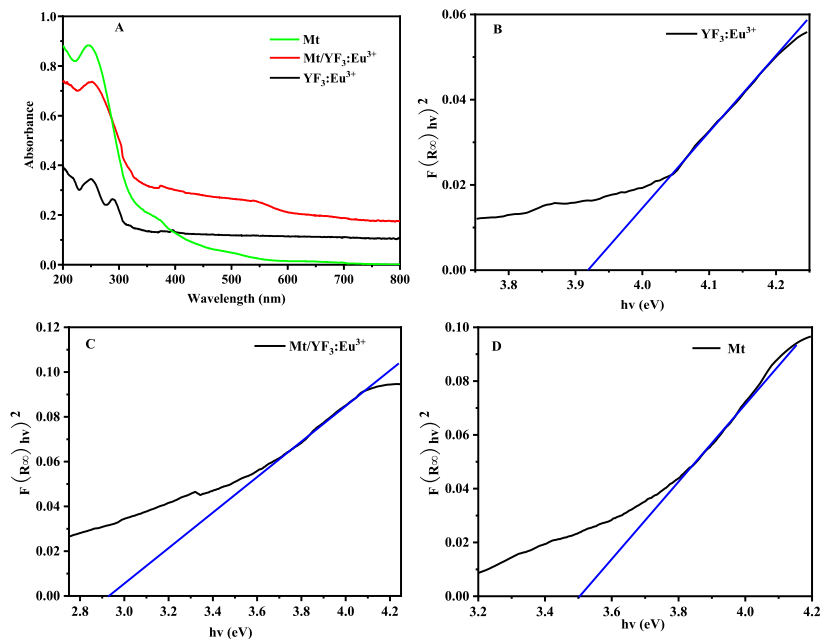


Fig. 9. (A) UV-vis spectra of Mt, Mt/YF₃:Eu³⁺ and YF₃:Eu³⁺ nanocomposite; (B–D) DRS spectra of YF₃:Eu³⁺, Mt/YF₃:Eu³⁺ and Mt nanocomposite with the corresponding plots of $[F(R_{\infty})/hv]^2$ versus $h\nu$.

or momentum is transferred by collision to another electron or another hole, and the recombination process that causing the electron or hole transition is called Auger recombination. According to the reported literature, the dielectric confinement effect between Mt and YF₃:Eu³⁺

nanoparticles could enhanced the local field strength of the crystals, thereby will boosting the luminescence property of the YF₃:Eu³⁺ nanoparticles. Owing to the influence of the crystal field in the solid material system, only the rare earth ions (Eu³⁺) doped in the matrix

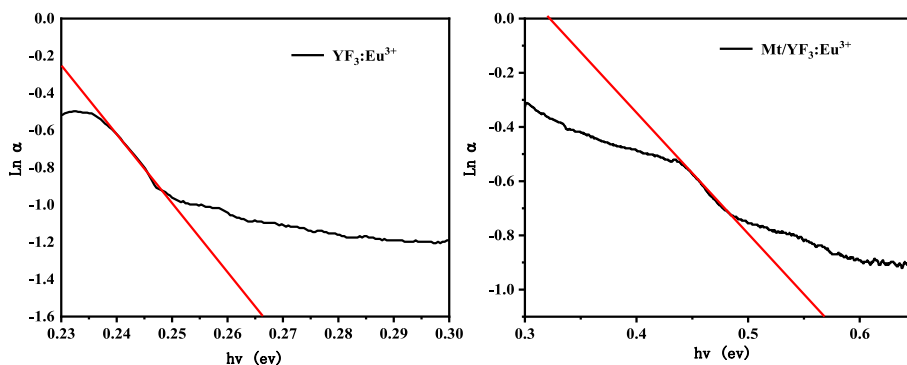


Fig. 10. Urbach tail energy fitting of $\text{YF}_3:\text{Eu}^{3+}$ and $\text{Mt}/\text{YF}_3:\text{Eu}^{3+}$ nanocomposite.

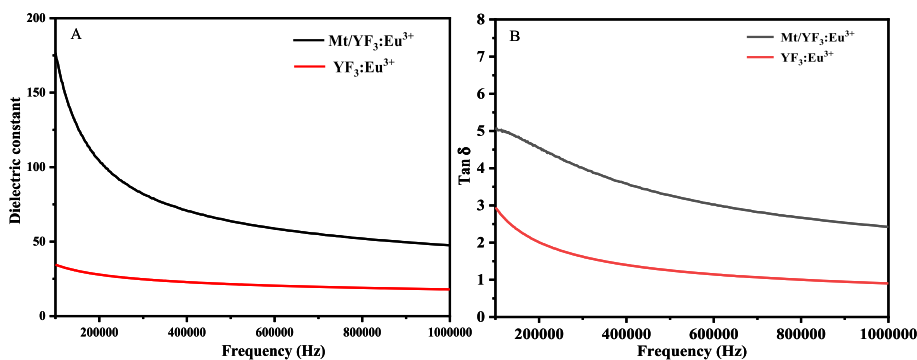


Fig. 11. Dielectric performance of $\text{YF}_3:\text{Eu}^{3+}$ and $\text{Mt}/\text{YF}_3:\text{Eu}^{3+}$; (A) dielectric constant and (B) $\tan \delta$

lattice were excited to produce radiation transitions. But the rare earth ions (Eu^{3+}) exposed on the surface of the matrix material or close to the surface of the matrix material were difficult to be excited [21]. The combination Mt and $\text{YF}_3:\text{Eu}^{3+}$ could enhance the intensity of the local field on the surface of matrix (YF_3), thus the rare earth ions (Eu^{3+}) on the matrix surface are activated and become easily excited, thereby increased the concentration of exciting state rare earth ions (Eu^{3+}) [22], and then enhanced the luminescence intensity of $\text{Mt}/\text{YF}_3:\text{Eu}^{3+}$ nanocomposite. Compared with the method of enhancing the luminescent property of rare earth luminescent materials through the doped method and core-shell structure strategy [23,27], the method of Mt as the carrier is more suitable for optimizing luminescent property of rare earth luminescent materials.

4. Conclusions

Novel silicate clay minerals-based $\text{Mt}/\text{YF}_3:\text{Eu}^{3+}$ nanocomposites were prepared by one step precipitation method. The combination of Mt and $\text{YF}_3:\text{Eu}^{3+}$ not only gives Mt to luminescence properties but also optimized the luminescence intensity, quantum yield and lifetime of $\text{YF}_3:\text{Eu}^{3+}$ nanoparticles by regulate their size, exciton binding energy and band gaps. A new type of $\text{Mt}/\text{YF}_3:\text{Eu}^{3+}$ nanocomposite have application prospects in lighting lamps, displays, imaging and drug delivery fields. The preparation method is simple process, high yield, and mild reaction conditions. This research provided a new method for the preparing a new type of silicate clay minerals-based nanocomposites.

Author contribution

Hongxia Peng and Jingyou Jiang conceived and designed the experiments, and Hongxia Peng and Junna Xu supervised the research; Juan Zhu and Huibin Shi performed the synthesis and characterization, interpreted the data and wrote the paper with help from Weicai Peng and Fabio Yu.

Declaration of competing interest

The authors declared that they have no conflicts of interest to this work. We declare that we do not have any commercial or associative interest that represents a conflict of interest in connection with the work submitted.

Acknowledgements

This work was supported by Hunan Natural Science Foundation of China (grant number 2022JJ30315); the Natural Science Research Talent Project of Hainan Medical University (Grant JBG202101); Hainan Province Clinical Medical Center (2021) Project for Functional Materials and Molecular Imaging Science Innovation Group of Hainan Medical University; the Scientific research project of Hunan province department of education (20B323).

References

- [1] J. Xie, W.B. Hu, D. Tian, Selective growth and upconversion photoluminescence of Y-based fluorides: from $\text{NaYF}_4:\text{Yb}/\text{Er}$ to $\text{YF}_3:\text{Yb}/\text{Er}$ crystals, *Nanotechnology* 31 (2020) 505–605.
- [2] D. Hu, H.X. Peng, Y.X. Peng, Synthesis and enhanced luminescence properties of $\text{CuS}/\text{YF}_3:\text{Eu}$ core-shell nanoparticles, *Appl. Phys. A* 126 (2020) 385–395.
- [3] C.Y. Wang, X.Q. Mu, J. Huo, Highly-efficient SERS detection for E. coli using a microfluidic chip with integrated $\text{NaYF}_4:\text{Yb},\text{Er}/\text{SiO}_2/\text{Au}$ under near-infrared laser excitation, *Microsyst. Technol.* (2020) 1–7.
- [4] X.Y. Cui, H.Y. Wu, T.J. Hu, Pressure effect on the ionic transport behavior and dielectric property of YF_3 , *J. Alloys Compd.* 823 (2020) 10–19.
- [5] H. Lin, D.Q. Chen, Y.L. Yu, Ultraviolet upconversion luminescence of Gd^{3+} and Eu^{3+} in nano-structured glass ceramics, *Mater. Res. Bull.* 47 (2) (2012) 469–472.
- [6] L.H. He, X. Li, Y. Yang, Morphology-controlled synthesis, growth mechanism and fluorescence of $\text{YF}_3:\text{Eu}^{3+}, \text{Bi}^{3+}$, *Mater. Res. Bull.* 95 (2017) 483–490.
- [7] X.L. Lei, R.F. Li, D.T. Tu, Intense near-infrared-II luminescence from $\text{NaCeF}_4:\text{Er}/\text{Yb}$ nanoprobes for in vitro bioassay and in vivo bioimaging, *Chem. Sci.* 9 (2018) 4682–4688.
- [8] M. Darbandia, Thomas Nann, One-pot synthesis of $\text{YF}_3/\text{silica}$ core/shell nanoparticles, *Chem. Commun.* (2006) 776–778.

- [9] G.X. Liu, S.D. Zhang, X.T. Wang, Hydrothermal synthesis and property comparison of $\text{YF}_3:\text{Eu}^{3+}$ luminescent nanomaterials with various morphology, *Hua Hsueh Hsueh Pao* 68 (2010) 1298–1302.
- [10] Y.L. Wang, F. Hong, L.Y. Yu, Construction, energy transfer, tunable multicolor and luminescence enhancement of $\text{YF}_3:\text{RE}^{3+}$ (RE=Eu,Tb)/carbon dots nanocomposites, *J. Lumin.* 221 (2020) 1–10.
- [11] H. Yin, Y. Kuwahara, K. Mori, Plasmonic metal/ $\text{Mo}_x\text{W}_{1-x}\text{O}_{3-y}$ for visible-light-enhanced H_2 production from ammonia borane, *J. Mater. Chem. A* (2018) 6–15.
- [12] Z. Hu, C. Fang, B. Li, First-in-human liver-tumour surgery guided by multispectral fluorescence imaging in the visible and near-infrared-I/II windows, *Nat. Biomed. Eng.* 4 (2020) 259–271.
- [13] Y.X. Liu, S.S. Liu, H.X. Peng, Structural design and synthesis of new MoO_{3-x} interlayer bi-functional nanomaterials for enhanced up-conversion luminescence properties, *Adv. powder tech.* 32 (2021) 2053–2063.
- [14] M. Wang, Z. Yang, Y.F. Wang, Preparation and characterization of $\text{NaGdF}_4:\text{Eu}^{3+}/\text{AAO}$ thin films, *Chem. J. Chin. Univ.* 32 (5) (2011) 1037–1042.
- [15] H.X. Peng, D. Wu, H. Wan, Facile synthesis and characterization of halloysite@ $\text{W}_{18}\text{O}_{49}$ nanocomposite with enhanced photocatalytic properties, *Appl. Clay Sci.* 183 (2019) 105319–105327.
- [16] K. Liu, W.Y. Li, S.T. Chen, The design, fabrication and evaluation of 3D printed HNTs/MgO whiskers/PLLA composite scaffold with honeycomb microstructure for bone tissue engineering, *Compos. Part B: Eng.* (2020) 192.
- [17] W. Ge, Q.L. Ma, Z. Ai, Three-dimensional reduced graphene oxide/montmorillonite nanosheet aerogels as electrode material for supercapacitor application, *Appl. Clay Sci.* (2021) 206.
- [18] W. Guo, W. Liu, Li Xu, Halloysite nanotubes loaded with nano silver for the sustained-release of antibacterial polymer nanocomposite scaffolds, *J. Mater. Sci. Technol.* 46 (11) (2020) 45–53.
- [19] K. Lim, W.S. Chow, S.Y. Pung, Enhancement of thermal stability and UV resistance of halloysite nanotubes using zinc oxide functionalization via a solvent-free approach, *Metall. Mater. Trans. A. Phys. Metall. Mater. Sci.* 26 (6) (2019) 787–795.
- [20] K. Ravichandran, E. Sindhuja, Fabrication of cost effective g- C_3N_4 -Ag activated ZnO photocatalyst in thin film form for enhanced visible light responsive dye degradation, *Mater. Chem. Phys.* 221 (2019) 203–215.
- [21] C. Gong, Q.J. Li, Ran Liu, Structural phase transition and photoluminescence properties of $\text{YF}_3:\text{Eu}^{3+}$ nanoparticles under high pressure, *Phys. Chem. C* 118 (39) (2014) 22739–22745.
- [22] S. Li, P. Wu, H. Li, Synthesis and characterization of organo-montmorillonite supported iron nanoparticles, *Appl. Clay Sci.* 50 (3) (2010) 330–336.
- [23] W.P. Chen, Y.J. Ouyang, M. Mo, Observation of energy transfer from Eu^{2+} to Eu^{3+} and tunable luminescence in phosphors $\text{YF}_3:\text{Eu}$ prepared by hydrothermal method, *J. Lumin.* 229 (2021) 117672–117682.
- [24] S. Zhao, Y.X. Li, Q.Y. Liu, An orally administered CeO_2 @Montmorillonite nanozyme targets inflammation for inflammatory bowel disease therapy, *Adv. Funct. Mater.* 30 (2020) 2004692–2004706.
- [25] Y.L. Lin, X. Gao, J.P. Yue, A soil-inspired dynamically responsive chemical system for microbial modulation, *Nat. Chem.* 15 (2023) 119–128.
- [26] W.J. Guan, S. Wang, C. Lu, Fluorescence microscopy as an alternative to electron microscopy for microscale dispersion evaluation of organic–inorganic composites, *Nat. Commun.* 7 (2016) 11811–11818.
- [27] Y. Wu, D.M. Yang, X.J. Kang, Core-shell structured luminescent and mesoporous $\beta\text{-NaYF}_4:\text{Ce}^{3+}/\text{Tb}^{3+}$ @ mSiO_2 -PEG nanospheres for anti-cancer drug delivery, *Dalton Trans.* 42 (2013) 9852–9861.
- [28] X.Y. Cui, H.Y. Wu, T.J. Hu, Pressure effect on the ionic transport behavior and dielectric property of YF_3 , *J. Alloys Compd.* 823 (2020) 10–19.
- [29] M. Zhao, P. Liu, Halloysite nanotubes/polystyrene (hnts/ps) nanocomposites via in situ bulk polymerization, *J. Therm. Anal. Calorimetry* 94 (1) (2008) 103–107.
- [30] C.D. Qin, J.J. Tang, R.X. Qiao, S.J. Lin, Tetracycline sensitizes TiO_2 for visible light photocatalytic degradation via ligand-to-metal charge transfer, *Chin. Chem. Lett.* 33 (2022) 5218–5222.
- [31] J. Jagielski, S. Kumar, W.Y. Yu, C.J. Shih, Layercontrolled two-dimensional perovskites: synthesis and optoelectronics, *J. Mater. Chem. C* 5 (2017) 5610.
- [32] J.T. Lin, C.C. Liao, C.S. Hsu, Harnessing dielectric confinement on tin perovskites to achieve emission quantum yield up to 21, *J A C S* 6 (2019) 1–9.
- [33] Y.Z. Jiang, M.H. Cui, S.S. Li, Reducing the impact of Auger recombination in quasi-2D perovskite light-emitting diodes, *Nat. Commun.* 12 (2021) 336–346.